IEEE Access
Multidisciplinary ⋮ Rapid Review ⋮ Open Access Journal

Received October 6, 2019, accepted October 28, 2019, date of publication October 31, 2019, date of current version November 13, 2019.

Digital Object Identifier 10.1109/ACCESS.2019.2950689

Performance Comparison of Adaptive Mechanisms of Cleaning Module to Overcome Step-Shaped Obstacles on Façades

JOOYOUNG HONG[1], (Student Member, IEEE), GARAM PARK[2], JISEOK LEE[2], JONGWON KIM[1], HWA SOO KIM[3], (Member, IEEE), AND TAEWON SEO[2], (Member, IEEE)

[1]School of Mechanical and Aerospace Engineering, Seoul National University, Seoul 08826, South Korea
[2]School of Mechanical Engineering, Hanyang University, Seoul 04763, South Korea
[3]School of Mechanical System Engineering, Kyounggi University, Suwon 16227, South Korea

Corresponding authors: Hwa Soo Kim (hskim94@kgu.ac.kr) and TaeWon Seo (taewonseo@hanyang.ac.kr)

This work was supported in part by the National Research Foundation of Korea (NRF) Grant funded by the Ministry of Science and ICT of the First-Mover Program for Accelerating Disruptive Technology Development under Grant 2018M3C1B9088331 and Grant 2018M3C1B9088332, and in part by the Human Resources Program in Energy Technology of the Korea Institute of Energy Technology Evaluation and Planning (KETEP) from the Ministry of Trade, Industry & Energy, South Korea, under Grant 20184030201970.

ABSTRACT As the demand and market for building maintenance are increasing, automated building façade cleaning has become essential. Robots are replacing human workers because cleaning work on high-rise buildings using gondolas can be dangerous. Several façade cleaning robots have been developed for climbing, and practical knowledge to clean the façade is being adopted in their cleaning devices. In this study, a passive linkage suspension mechanism and tri-star wheels are applied to solve the problems of unclean zones due to failures during overcoming obstacles and the problems through the use of additional actuators. Various mechanism models have been introduced and their performances have been compared based on dynamic simulation considering obstacle encounters.

INDEX TERMS Façade cleaning, cleaning device, cleaning module, skyscrapers, passive linkage suspension.

I. INTRODUCTION

In recent years, cleaning buildings has become a significant issue for many people. In countries like China, Hongkong, and some countries in Middle Asia, the number of buildings is rapidly increasing with the developments in construction technology [1]. Therefore, the demand for cleaning and maintaining building façade has significantly increased. Façade and windows are contaminated by sand and fine dust owing to environmental pollution, and cleaning them involves high risk because human workers suspend themselves at great heights.

To reduce this risk, many works have introduced substitute robotic devices [24]. Skypro and IPC Eagle use the propulsion force of propellers to attach themselves on the façade [2], [3], and clean it using brush and water. GEKKO robots use suction pads with tracks to move on the façade [4]. GEKKO Façade is a mobile-based robot and GEKKO Gondola has suction pads with tracks that can be used with various building maintenance units (BMUs). BWMR (Building wall maintenance robot) uses guide rails equipped on the buildings [5]. It has nozzles, squeegees, and suction parts to clean the façade. Unmanned high-rise façade cleaning robot (FCR-M1) has been developed and implemented on a gondola to be used in BMUs [6]. FCR-M1 is mounted on a bracket in a gondola, and cleans the façade using the cleaning device equipped with squeegees, nozzles, brush, and suction parts.

From the performance perspective, these cleaning robots have problems with negotiating the façade frame, or use additional actuators to overcome the frame using complicated control methods. GEKKO has no negotiating performance because the suction pads have to normally maintain contact with the surface. Skypro and IPC Eagle overcome obstacles by controlling the propeller speed. This control has slow response owing to the inertia of the propellers, and their speed must be changed beforehand. BWMR overcomes obstacles by lifting 2-DOF squeegees. However, for

The associate editor coordinating the review of this manuscript and approving it for publication was Okyay Kaynak.

the efficient working of BWMR, buildings must be installed with guide rails, which proves to be a limitation to this method. FCR-M1 has a 2-DOF manipulator that can avoid a frame vertically and rotate in the yaw direction. In the field test on a building [6], there are uncleaned areas around frame.

In this study, these limitations and problems have been solved by adopting mechanisms from robots that overcome obstacles and rough terrain. Shrimp rover has parallelogram links and spoked legs with spring, and can climb step-like obstacles [7]. Its spoke leg rising trajectory is calculated and it can climb steps over 1.5 times the height of its wheels. Crab rover has two parallelogram links that are articulated with each other [8]. Using this articulated structure, the rover can climb step-like obstacles and maintain a horizontal posture while passing a raised spot and a dent. Robots with the rocker-bogie mechanism are also popular and many researchers have developed and optimized such robots to improve the climbing ability [9]. The rocker-bogie mechanism is a typical passive linkage suspension to locomote on rough terrain. However, this mechanism has a serious problem; when the rear wheels are climbing the steps, the middle wheels remain in the air. Researchers solved this problem by changing the location of the pivot joint [10]. Additionally, there is a modular robot whose compliant components are situated on the joints between the modules [11]. This robot can climb up and down the steps because it consists of two springs on both sides of each joint. The wall cleaning platform has triangular tracks instead of wheels [12]. A rope ascender on the platform pulls up the platform and overcomes the obstacles on the buildings passively via these triangular tracks. TQTMR (Tiltable quad-tracked mobile robot) has four 2-DOF tracks that are articulated [13]. These 2-DOF tracks have high terrainability and maneuverability, and they are triangle-shaped, which helps in overcoming obstacles such as climbing steps.

This new adaptive cleaning module can passively overcome step-like obstacles without complicated control method by using the linkage suspension mechanism with the same four cleaning methods as in the FCR-M1. The main difference between this new adaptive cleaning module and the robots is the actuating method. The other robots mentioned above paragraph, except the wall cleaning platform, have actuators on the wheels or in the platform, and torque helps the robots overcome step-like obstacles using the friction force and traction force between the wheels and contact surfaces. Or, some robots use suction cups to adhere to the façade, and this needs complicated control and consumes more power. In contrast, this new adaptive cleaning module is located at the end-effector of the manipulator of FCR-M1 or other robotic platforms. There are no needs of actuators for overcoming the obstacles in this cleaning module. Therefore, this cleaning device passively overcomes the obstacles using passive linkage mechanisms or different wheel types.

The rest of the paper is organized as follows. In Section 2, the overall configuration and cleaning mechanism of the new adaptive cleaning module have been explained, and the performance comparison for different mechanisms have been introduced. This section also includes an analysis of the tri-star wheel, which is adopted instead of conventional wheels. In Section 3, indices for the comparisons are introduced and the dynamic simulation environment is explained. In Section 4, the details of dynamic simulation and the result have been explained. Section 5 consists of the conclusion and discussion.

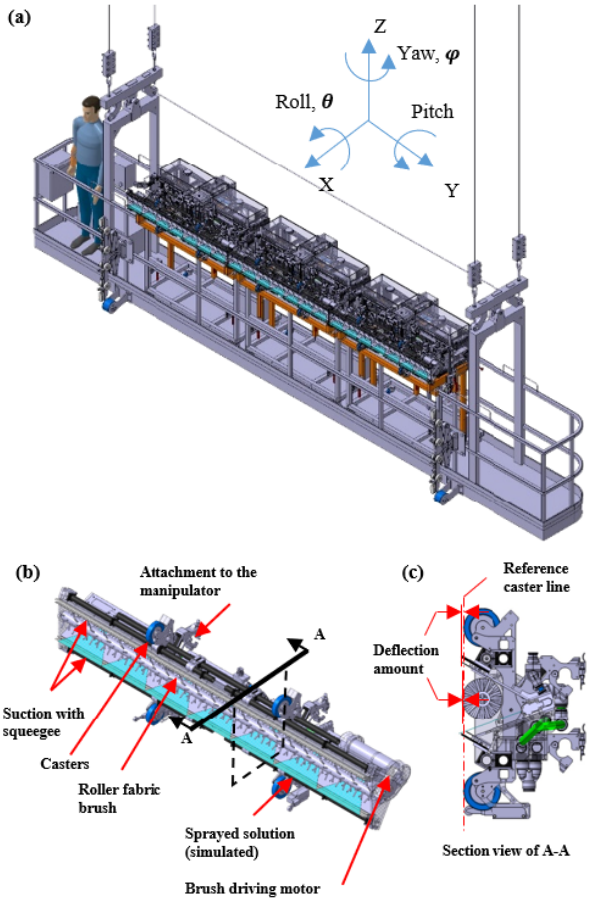

FIGURE 1. (a) Coordinate system of FCR-M1s on a gondola, and (b), (c) a cleaning module [6].

II. A NEW ADAPTIVE CLEANING MODULE

A. CLEANING MODULE

A cleaning module was developed, as shown in Fig. 1 [6]. This cleaning module was optimized using Taguchi's optimization method [14]. It consists of four cleaning parts. Sand dust and fine dust are swept away by spraying the cleaning solution. The roller fabric brush rotates and sweeps away the dust. Then, the dirty solution is squeegeed and suctioned by the upper and lower squeegees. The casters are used to maintain a distance from the façade so that the forces generated from the deflection of squeegees and roller fabric brush are maintained subsequently.

In [6], during the field test on 63 Building in South Korea, an uncleaned area remained on the façade (Fig. 2). Yoo et al. [6] explained that this occurred because the

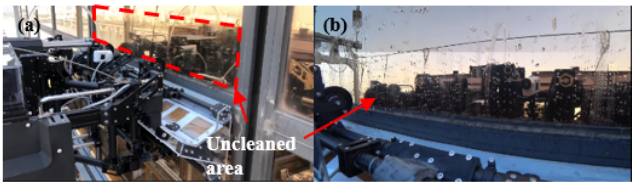

FIGURE 2. Uncleaned area of façade at the field test [6].

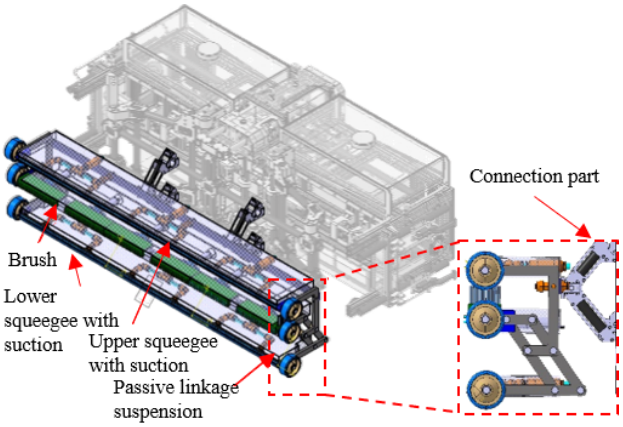

FIGURE 3. An example of a new adaptive cleaning module equipped on the FCR-M1.

FCR-M1 descends with the gondola at a constant speed. During the descent, the frame of façade is detected by the toggle switches under the cleaning module. When the frame is detected, the manipulator pulls the end-effector rapidly and the cleaning module avoids the frame. Because the cleaning module avoids collision, a trajectory is generated, thereby resulting in the uncleaned area. Additionally, the sudden rapid fall of manipulator from the façade causes significant changes in the acceleration and force, which are undesirable situations for the manipulator.

B. ADAPTIVE SUSPENSION LINKAGE MECHANISM

Section 2. A describes the problem related to the cleaning module. To solve the problem, a complex control method should be avoided, and a mechanical perspective should be instead considered. Many robots use the passive linkage suspension mechanisms to overcome obstacles. Because the robots are meant to establish stable locomotion on the rough terrain, their wheels maintain good contact with the surface. Some researchers suggest the use of linkage suspension mechanisms that help in climbing the step-like obstacles with better performance [16]–[18]. This characteristic can be applied to the new cleaning module.

The previous cleaning module can be divided into three parts, upper squeegee, roller brush, and lower squeegee. The nozzles might be turned off during overcoming the obstacles by being located on the connection part. For example, this new adaptive cleaning module is similar to Fig. 3 and can be equipped on the end-effector of FCR-M1 or other platforms.

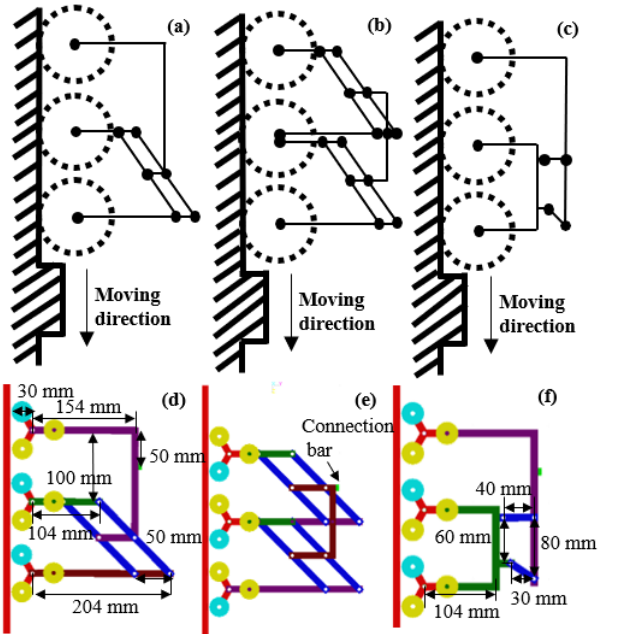

FIGURE 4. Schematic of linkage suspension, (a) RCL-E, (b) CRAB, (c) FBRB, and length specification ((d), (e), (f)).

As shown in Fig. 3, the cleaning parts are divided into three parts. Each cleaning part is connected to the co-axis with wheels to maintain contact with the surface until the wheel comes in contact with the frame. This reduces the uncleaned area when the façade cleaning robot passes the frame. This implies that as the wheel with the lower squeegee comes in contact with the frame, it climbs the frame while other wheels remain in contact with the façade. The wheel with the brush and that with the upper squeegee undergo a similar process.

For comparison, some specifications are shown in Fig. 4 (d), (e), and (f). The link length and number of wheels might be the same for the comparison [19]. Although there are many linkage mechanisms, the number of wheels of this cleaning module is six because the cleaning module is divided into three parts. Additionally, dimensions such as the length of linkage, wheel radius, location of connection bar, force from the manipulator, and contact condition should be the same.

The models chosen for comparison are RCL-E, CRAB, and the rocker-bogie mechanism with four-bar linkage (FBRB), whose schematics are shown in Fig.4. The rocker-bogie mechanism is a well-known Mars-rover suspension that can move efficiently on rough terrain. It can overcome obstacles higher than its wheel size. CRAB rover has two articulated parallelogram linkages and RCL-E has one with rocker linkage. The parallelogram linkages rotate about the pivot of the center of rotation, maintaining the verticalness of the linkage with the wheel. These parallelogram linkages are inclined to the surface such that the climbing ability of the model is increased (Fig. 5). In Fig. 5, the pivot joint of the wheel with lower squeegee is the point of intersection of the dotted line with the same slope as the parallelogram linkage,

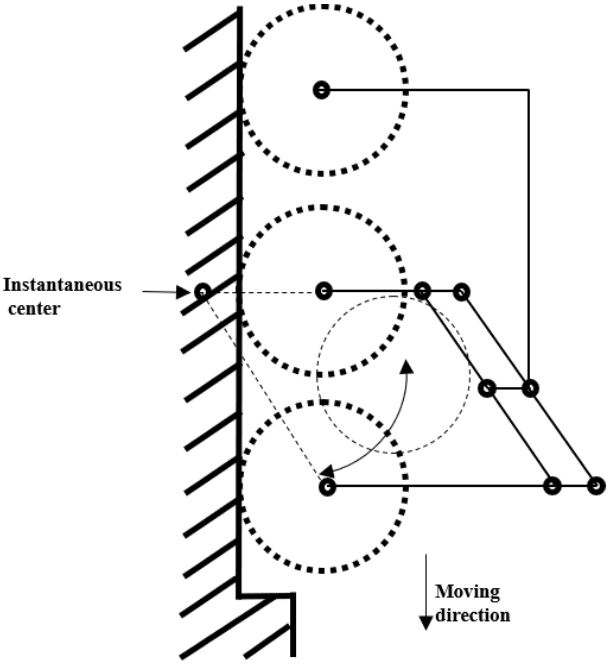

FIGURE 5. Wheel lifting trajectory by changing instantaneous center of RCL-E.

having the same length from the center of the wheel, and the dotted extended line of other wheels. The wheel rotates about this pivot joint and the trajectory of the wheel is shown in Fig. 5. This change of pivot joint makes the linkage mechanism avoid the singular point when the parallelogram linkages are parallel to the surface.

C. DESIGN OF TRI-STAR WHEEL

To increase the ability of passively climbing step-like obstacles, tri-star wheels are adopted instead of conventional wheels. Although changing the location of the pivot joint makes a positive momentum for the linkage to climbing obstacles, there is a limitation that the possible angle range is small and the distance between the pivot joint and the center of the wheel is eventually short. The change in the momentum is relatively smaller than the change in the angle. To complement the momentum, tri-star wheel is adopted, which is designed to prevent the interference and collision between the wheel frame and the façade frame (Fig. 6). Some studies have investigated the design of tri-star wheel for step climbing [20], [21].

The façade frame consists of just one step. Therefore, the design variables are t, R, r. The design variable R is the wheel frame radius, t is the thickness of the wheel frame, t_{max} is the maximum thickness of the wheel frame, r is the radius of the wheel, r_{min} is the minimum radius of the wheel, h is the height of the frame, and θ_h is the angle between the dotted line, which connects the centers of two wheels (one under the frame and the other on the frame and the façade). Line 1 connects the centers of the wheel under the frame and the wheel frame, and Line 2 is t_{max} away from line 1 and

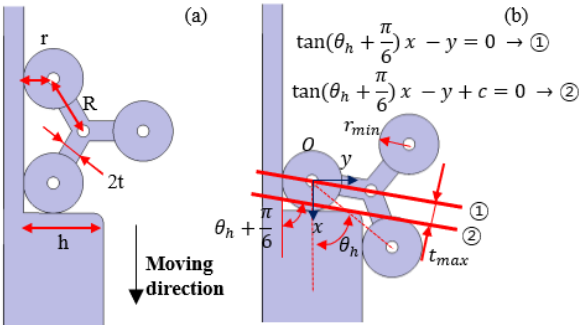

FIGURE 6. Tri-star wheel design variables.

passes the edge of the façade frame. When the center of the wheel under the frame is the origin of a coordinate, the x- and y-coordinates of the edge are (r, h-r), respectively. From the geometry of the tri-wheel and the frame, t_{max}, θ_h, and r_{min} are calculated.

$$\theta_h = \sin^{-1}\frac{h}{\sqrt{3}R} \tag{1}$$

The equations of Lines 1 and 2 are respectively given by

$$\tan(\theta_h + \frac{\pi}{6})x - y = 0 \tag{2}$$

$$\tan(\theta_h + \frac{\pi}{6})x - y + c = 0 \tag{3}$$

where $\pi/6$ is owing to the triangular shape of the tri-wheel frame and c is a constant. The distance between two lines, which is the maximum thickness of the wheel frame, is given by

$$t_{max} = \frac{\left|r\left(\tan\left(\theta_h + \frac{\pi}{6}\right) + 1\right) - h\right|}{\sqrt{(\tan(\theta_h + \frac{\pi}{6}))^2 + 1}} \geq t \tag{4}$$

From equation (4), r_{min} can be derived as:

$$r_{min} = \frac{h + t\sqrt{(\tan(\theta_h + \frac{\pi}{6}))^2 + 1}}{(\tan\left(\theta_h + \frac{\pi}{6}\right) + 1)} \tag{5}$$

The dynamic simulation will be introduced in Section 3. The height of the façade frame will be 15, 30, and 40 mm. Therefore, h_{max} is 40 mm, t is 5 mm, and R is 30 mm. Substituting the values into (1) and (5), θ_h is 50.3° and r_{min} is 10.15 mm. For the simulation, the radius of the wheel is 15 mm.

D. PARAMETRIC DESIGN OF LINKAGE

For the comparison models, the parameters of linkages are shown in Fig. 7. In the RCL-E model, l_r, l_s, and l_l are important linkage parameters. L_r, L_f, and θ_0 denote the distance between the rear wheel and middle wheel, the distance between the front wheel and middle wheel, and the angle between the parallelogram linkage and vertical linkage, respectively. θ_0, θ_d, and θ_h denote the initial angle, the angle between the façade and the dotted line connecting the front wheel and middle wheel, and the angle between the linkage

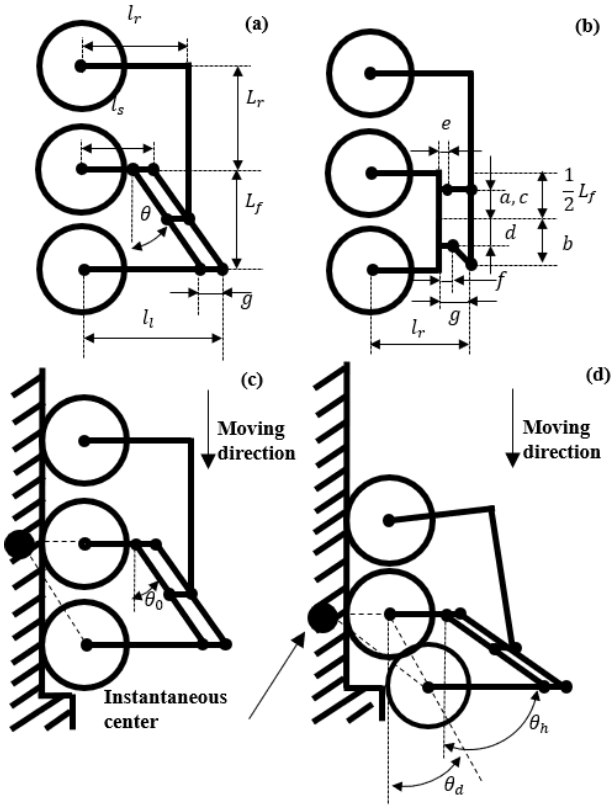

FIGURE 7. Parameters of linkages ((a) RCL-E and (b) FBRB) and (c), (d) diagrams of RCL-E when the front wheel overcomes an obstacle.

of the parallelogram and the façade, respectively.l_h, l_l, l_s, and l_r denote the lengths of parallelogram linkage, front long linkage, middle short linkage, and the height of rear rocker linkage, respectively. r, h, and$g$ denote the radius of the wheel, the height of an obstacle, and the distance between two parallelogram linkages, respectively. Some parametric relationships are as follows:

$$\theta_0 = \tan^{-1}\frac{(l_l - l_s)}{2L_f} \tag{6}$$

$$l_h = \frac{L_f}{\cos\theta_0} \tag{7}$$

$$\theta_h = \sin^{-1}\frac{(l_l - l_s + h)}{l_h} \tag{8}$$

$$\theta_d = \theta_h - \theta_0 \tag{9}$$

In Fig. 7(d), considering the interference of each wheel, there should be a constraint as follows:

$$\frac{h}{\sin\theta_d} \geq 2r \tag{10}$$

In Fig. 7 (b), the parameters of the linkages are the followings: a, b, c, d, e, f, and g are the parameters from the front bogie. All lengths of the RCL-E, CRAB, and FBRB models are summarized in Fig. 4 (d), (e), and (f). In this study, l_r, L_f, and L_r are dimension from the cleaning module for the comparison [6], and L_f and L_r are selected as the same length. Additionally, the value of θ_0 is 45°.

III. COMPARISON WITH DYNAMIC SIMULATION

A. PERFORMANCE INDICES

There are various performance indices to measure the abilities of a robot. D. Apostolopoulos mentioned three performance indices for wheeled robots [22]: trafficability, maneuverability, and terrainability. Because there are no other desired trajectories, the maneuverability is not suitable for this comparison. Additionally, there are no actuators on the wheels and the façade is rigid enough to ignore sinkage. Therefore, trafficability is not suitable for this comparison either. Because these adaptive cleaning modules are designed to overcome obstacles, the terrainability index is a suitable parameter for comparison.

In the terrainability category, many performance indices have been proposed. Among those indices, the direction of the x-coordinate and yaw direction movement is related to the parallel 2-DOF manipulator [23]. Because the manipulator is 2-DOF for x-coordinate and yaw direction in Fig. 1(a), the change of position and force are disturbances.

For stable cleaning tasks and safety of the human operator, disturbance is an undesirable component. Choi. et al. proposed a new terrainability index as PVI (posture variation index) and compared wheeled mobile platforms. Because there are no mechanical components for suspension, such as springs and dampers, the variation in the direction of x-coordinate is inevitable and thus, PVI is not suitable for this study. It should be noted that the posture variation of direction in the x-coordinate can be coped with the manipulator.

The acceleration of this adaptive cleaning module is related to the sudden change in the load for the robot. If the accelerations in the directions of x-coordinate and yaw are large, more manipulation occurs due to the inertia of the cleaning module.

While overcoming obstacles, the force dramatically changes at the moment of attachment and detachment [6]. It is very dangerous because the gondola and the manipulator could diverge, and the façade and the robot can be damaged. Moreover, the actuators can be saturated by the limitation of the specification of the actuators. As the gondola is descending along the – z-direction and the manipulator has no DOF along the roll direction, it is critical to the robot and the gondola if there are forces and acceleration in the roll direction. Note that there are rotation joints in the connection parts as shown in Fig. 3. By these rotation joints, this cleaning module has a degree of freedom in pitch direction, and the stability in that direction is not considered.

In this study, the terrainability and rolling stability index (RSI) are introduced to examine the safety and stable overcoming performance. Terrainability is measured via the acceleration of the x-coordinate and the yaw direction. The RSI is measured from the acceleration of the roll direction.

1) TERRAINABILITY

Terrainability, in this study, is defined in two directions, x-coordinate and yaw. Terrainability in the direction of x-coordinate is measured from the RMS value of the

acceleration of x-coordinate of the adaptive cleaning module while overcoming the obstacle, and can be derived as follows:

$$TA_x = \sqrt{\frac{1}{N}\sum_{i=1}^{N}(\ddot{x}_i)^2} \tag{11}$$

where $\ddot{x}_i$ is the acceleration of the adaptive cleaning module in the direction of x-coordinate at the i-th step in a simulation. And N is the total number of simulation steps.

Terrainability in the direction of yaw is measured from the RMS value of the acceleration of yaw direction of the adaptive cleaning module, and can be derived as follows:

$$TA_\varphi = \sqrt{\frac{1}{N}\sum_{i=1}^{N}(\ddot{\varphi}_i)^2} \tag{12}$$

where $\ddot{\varphi}_i$ is the acceleration in the direction of yaw of the adaptive cleaning module at the i-th step in a simulation.

If both TA_x and TA_φ are small, the obstacle overcoming performance is good and the robots with the adaptive cleaning module and the human operator are safe. Additionally, the smaller values reduce the size of the actuators and energy consumption during the cleaning tasks.

2) ROLLING STABILITY INDEX

RSI is the performance index for safety during descending along the –z-direction. RSI is measured from the RMS value of the acceleration of the adaptive cleaning module in the direction of roll, and can be derived as follows:

$$RSI = \sqrt{\frac{1}{N}\sum_{i=1}^{N}(\ddot{\theta}_i)^2} \tag{13}$$

where $\ddot{\theta}_i$ is the acceleration in the direction of the roll of the adaptive cleaning module at the i-th step in a simulation. Although the weight of the gondola is relatively smaller than the payload, it is still dangerous for the structure of the robot. This is the reason why the RSI value should be small because then it ensures safety for both the robot and the gondola with the human operator.

B. SIMULATION ENVIRONMENT

The performance comparison for models selected in Section 2. B is conducted using a dynamic simulation tool. The terrainability and RSI values are obtained from the dynamic simulation results. While descending, a gondola descends at constant speed, hanging on wires, and a robot is mounted on the gondola. A cleaning module is equipped at the end of the robot with the revolute joint, which has 1-DOF.

In the simulation, the comparison models have tri-star wheels with linkage mechanism suspension. Each model consists of two linkage mechanisms and a 1000mm- connection bar. In a realistic situation, it is important to set the contact conditions between the wheels and façade surface because the descending speed is set as the gondola speed, 7 m/min, which is very fast. The obstacles are 15, 30, and 40 mm in height. For simulations of the 15 mm obstacle, the simulation time and steps are 4.5 s and 9000, respectively. For simulations of both the 30- and 40- mm obstacles, the simulation time and steps are 5 s and 10000, respectively. The force is set as 10 N. Because up to 12 wheels are in contact with the façade surface simultaneously, the stiffness and damping coefficient for the contact conditions are selected as 1000 N/mm and 5 N/mm·s, respectively. The dynamic friction coefficient is 0.8 as the friction coefficient between glass and urethane ranges from 0.4 ∼ 0.8. For the contact surface tolerance factor, the base surface is 5.e-5, and the action surface is 3.e-5.

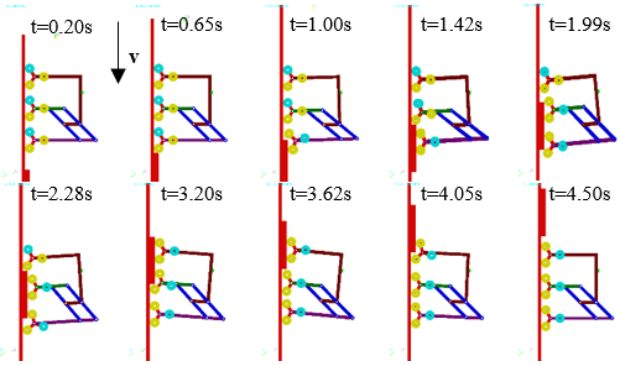

FIGURE 8. Simulation snapshots of RCL-E overcoming 15 mm obstacle.

TABLE 1. Obstacle overcoming ability.

Model		RCL-E	CRAB	FBRB
Height	15 mm	○	○	○
	30 mm	○	△	X
	40 mm	○	△	X

IV. RESULT AND DISCUSSION

A. RESULT

From the simulation, it is evident that the comparison models can overcome obstacles with the same height. For example, Fig. 8 shows the simulation of RCL-E overcoming the 15 mm obstacle. Table 1 lists the performance of each model for overcoming the obstacles with varying heights. As shown in Table 1, RCL-E overcomes the 40 mm step-like obstacles. CRAB also overcomes the 40 mm obstacles. However, at the end of the simulation time in the cases of 30- and 40- mm obstacles, the posture of the model is unstable, and it might tumble over after a few seconds. The FBRB overcomes only the 15 mm obstacle and it turned over in the case of 30- and 40- mm obstacles. Other mechanisms, which are not compared in this paper, are excluded because they did not overcome even the 15 mm obstacle.

As all three comparison models overcome the 15 mm obstacle, the terrainability and RSI are measured from only the 15 mm obstacle. The posture variation in the direction of x-coordinate is shown as Fig. 9 (a). It is evident that the posture variation of FBRB is the most dramatic and is the least for RCL-E. The deviation between the minimum and maximum height of RCL-E is less than 15 mm.

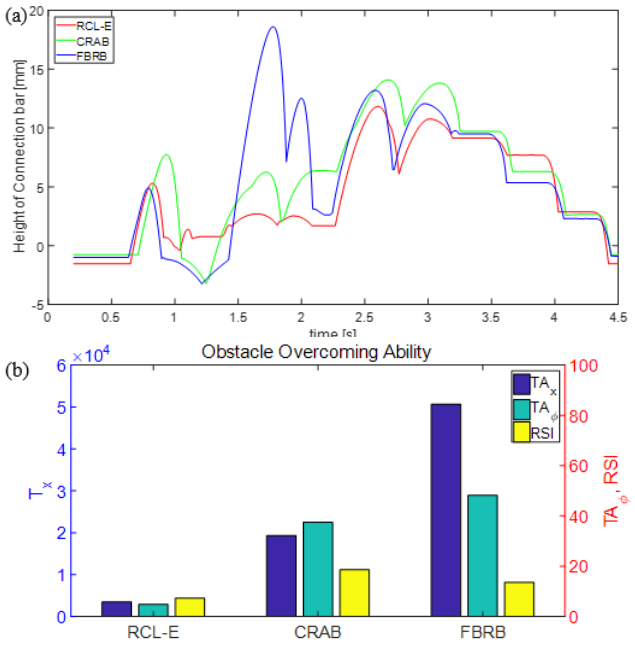

FIGURE 9. Simulation results during overcoming the 15 mm obstacle about (a) x-coordinate direction posture and (b) terrainability and RSI value bar graph about RCL-E, CRAB, and FBRB models.

TABLE 2. Terrainability and RSI value of three comparison models about 15 mm obstacle.

Model		RCL-E	CRAB	FBRB
Index	TA_x	3.4×10^{3}	2.0×10^{4}	5.1×10^{4}
	TA_φ	4.8	3.8×10^{1}	4.8×10^{1}
	RSI	7.3	1.9×10^{1}	1.4×10^{1}

Therefore, the ability of overcoming step-shape obstacle of RCL-E is good for the robot.

Fig. 9 (b) shows the bar graph of the obstacle overcoming ability of the three models. In Fig. 9 (a), a drastic change can be observed in the posture in relation to large acceleration. More sudden change in posture and larger acceleration results in bigger values of terrainability and RSI value. It should be noted that a fourth-order, low pass Butterworth filter was used for the acceleration results, whose cutoff frequency was the 100 Hz while the sampling frequency (calculated by the simulation time and steps) was 2000 Hz.

Some peak values occur because the cleaning modules met the obstacles that impacted them. As shown in Fig. 9 (b), RCL-E has the lowest terrainability and RSI values, while FBRB has the highest terrainability value, and CRAB has the highest RSI value. From the results, RCL-E is the most stable mechanism among these three models.

Table 3 shows the terrainability and RSI values of RCL-E overcoming the 15, 30, and 40 mm obstacles. If the obstacle is higher, the terrainability values increase. In contrast, the RSI values decrease for the higher obstacles. The results show

TABLE 3. Terrainability and RSI value of RCL-E among various height obstacles.

Height		15 mm	30 mm	40 mm
Index	TA_x	3.4×10^{3}	6.1×10^{3}	2.2×10^{4}
	TA_φ	4.8	8.5	1.3×10^{1}
	RSI	7.3	6.2	4.8

that the adaptive cleaning module accelerates more when it overcomes higher obstacles.

B. DISCUSSION

It is evident from the results that RCL-E shows the best stability in terrainability and RSI among the three models when overcoming the obstacles. For the 15 mm obstacle, the value of terrainability for RCL-E is less than 20% and 10% for CRAB and FBRB, respectively. For the cleaning tasks, lesser variations in acceleration in the two directions are good for the manipulation and cleaning performance, as mentioned by the author in [23].

For the point of rolling view, RCL-E also shows the least rolling while overcoming the obstacles (38% and 52% less than CRAB and FBRB, respectively). Because the RSI is related to the safety of the robot and gondola, RCL-E is more reliable than the other two models.

From Table 3, it is evident that the terrainability increases and RSI decreases as the height of obstacles increases. To overcome the obstacles, the cleaning module should lift wheels higher because the obstacles are higher. This implies that the cleaning module should lift with higher acceleration because the cleaning module descends with the same speed. In contrast, as the RSI value decreases, the wheels are stuck on the obstacles, and these situations cause the wheels to roll over. To develop stable adaptive cleaning modules, the wheels should be small, and the parameters of linkages should be larger to overcome higher obstacles stably.

V. CONCLUSION

It is difficult to overcome the obstacles in façades using conventional cleaning devices because there is no degree of freedom. To overcome the obstacles, this study proposed a passive linkage mechanism with tri-star wheels that can be integrated with various cleaning devices. The tri-star wheels were analyzed and designed to avoid interference between the wheel frames and obstacles. Next, the following models were chosen to compare their performances: RCL-E, CRAB, and the rocker-bogie mechanism with a four-bar linkage. In this paper, the performance indices, terrainability, and RSI have been introduced for the performance comparison. Dynamic simulations were conducted on these models for obstacles of varying heights. According to the results, RCL-E overcame obstacles with the height of up to 40 mm, which shows the best result among the three models. Because the obstacle had more height, the terrainability values were higher,

thereby indicating the need for more power. Additionally, the RSI value was lower, implying more stability against obstacles. For future work, this RCL-E model will be adopted to the novel cleaning module mechanism and the adaptive cleaning module will be equipped with the FCR-M1.

REFERENCES

[1] The Skyscraper Center. *The Global Tall Building Database of the CTBUH*. Accessed: Sep. 1, 2019. [Online]. Available: http://www.skyscrapercenter.com/countries

[2] SkyProCy Ltd. *SkyPro Cyprus*. Accessed: Sep. 1, 2019. [Online]. Available: http://www.skyprocy.com/en/company-en

[3] Highrise. *IPC Eagle*. Accessed: Sep. 1, 2019. [Online]. Available: http://www.ipceagle.com/products/highrise

[4] Gecko. *Serbot*. Accessed: Sep. 1, 2019. [Online]. Available: https://www.serbot.ch/en

[5] Y.-S. Lee, S.-H. Kim, M.-S. Gil, S.-H. Lee, M.-S. Kang, S.-H. Jang, B.-H. Yu, B.-G. Ryu, D. Hong, and C.-S. Han, "The study on the integrated control system for curtain wall building façade cleaning robot," *Automat. Construct.*, vol. 94, pp. 39–46, Oct. 2018.

[6] S. Yoo, I. Joo, J. Hong, C. Park, J. Kim, H. S. Kim, and T. Seo, "Unmanned high-rise Façade cleaning robot implemented on a gondola: Field test on 000-building in Korea," *IEEE Access*, vol. 7, pp. 30174–30184, 2019.

[7] R. Siegwart, P. Lamon, T. Estier, M. Lauria, and R. Piguet, "Innovative design for wheeled locomotion in rough terrain," *Robot. Auton. Syst.*, vol. 40, nos. 2–3, pp. 151–162, 2002.

[8] T. Thueer, P. Lamon, A. Krebs, and R. Siegwart, "Crab-exploration rover with advanced obstacle negotiation capability," in *Proc. ESA Workshop Adv. Space Technol. Robot. Automat.*, Noordwijk, The Netherlands, 2006, pp. 1–8.

[9] D. Kim, H. Hong, H. S. Kim, and J. Kim, "Optimal design and kinetic analysis of a stair-climbing mobile robot with rocker-bogie mechanism," *Mechanism Mach. Theory*, vol. 50, pp. 90–108, Apr. 2012.

[10] D. Chugo, K. Kawabata, H. Kaetsu, H. Asama, and T. Mishima, "Step climbing omnidirectional mobile robot with passive linkages," *Proc. SPIE*, Saporo, Japan, vol. 6052, pp. 60520K-1–60520K-13, 2005.

[11] S. H. Turlapati, M. Shah, S. P. Teja, A. Siravuru, S. V. Shah, and K. K. Madhava, "Stair Climbing using a compliant modular robot," in *Proc. IEEE/RSJ Int. Conf. Intell. Robots Syst. (IROS)*, Hamburg, Germany, Sep. /Oct. 2015, pp. 3332–3339.

[12] T. Kim, Y. Jeon, S. Yoo, K. Kim, H. S. Kim, and J. Kim, "Development of a wall-climbing platform with modularized wall-cleaning units," *Autom. Construct.*, vol. 83, pp. 1–18, Nov. 2017.

[13] J. Kim, J. Kim, and D. Lee, "Mobile robot with passively articulated driving tracks for high terrainability and maneuverability on unstructured rough terrain: Design, analysis, and performance evaluation," *J. Mech. Sci. Technol.*, vol. 32, no. 11, pp. 5389–5400, 2018.

[14] J. Hong, S. Yoo, I. Joo, J. Kim, H. S. Kim, and T. Seo, "Optimal parameter design of a cleaning device for vertical glass surfaces," *Int. J. Precis. Eng. Manuf.*, vol. 20, no. 2, pp. 233–241, 2019.

[15] D. Choi, Y. Kim, S. Jung, J. Kim, and H. S. Kim, "A new mobile platform (RHyMo) for smooth movement on rugged terrain," *IEEE/ASME Trans. Mechatronics*, vol. 21, no. 3, pp. 1303–1314, Jun. 2016.

[16] B. Chen, R. Wang, Y. Jia, L. Guo, and L. Yang, "Design of a high performance suspension for lunar rover based on evolution," *Acta Astronautica*, vol. 64, pp. 925–934, May/Jun. 2009.

[17] W.-S. Eom, Y.-K. Kim, J.-H. Lee, G.-H. Choi, and E.-S. Sim, "Study on a suspension of a planetary exploration rover to improve driving performance during overcoming obstacles," *J. Astron. Space Sci.*, vol. 29, no. 4, pp. 381–387, 2012.

[18] C.-K. Woo, H. D. Choi, S. Yoon, S. H. Kim, and Y. K. Kwak, "Optimal design of a new wheeled mobile robot based on a kinetic analysis of the stair climbing states," *J. Intell. Robotic Syst.*, vol. 49, no. 4, pp. 325–354, 2007.

[19] T. Thueer, A. Krebs, R. Siegwart, and P. Lamon, "Performance comparison of rough-terrain robots—Simulation and hardware," *J. Field Robot.*, vol. 24, no. 3, pp. 251–271, 2007.

[20] M. M. Dalvand and M. M. Moghadam, "Stair climber smart mobile robot (MSRox)," *Auto. Robots*, vol. 20, no. 1, pp. 3–14, 2006.

[21] Y. Yang, H. Qian, X. Wu, G. Xu, and Y. Xu, "A novel design of Tri-star wheeled mobile robot for high obstacle climbing," in *Proc. IEEE/RSJ Int. Conf. Intell. Robots Syst.*, Oct. 2012, pp. 920–925.

[22] D. Apostolopoulos, "Analytic configuration of wheeled robotic locomotion," Ph.D. dissertation, Robot. Inst., Carnegie Mellon Univ., Pittsburgh, PA, USA, 2001.

[23] I. Joo, J. Hong, S. Yoo, J. Kim, H. S. Kim, and T. Seo, "Parallel 2-DoF manipulator for wall-cleaning applications," *Automat. Construct.*, vol. 101, pp. 209–217, May 2019.

[24] T. Seo, Y. Jeon, C. Park, and J. Kim, "Survey on glass and Façade-cleaning robots: Climbing mechanisms, cleaning methods, and applications," *Int. J. Precis. Eng. Manuf.-Green Technol.*, vol. 6, no. 2, pp. 367–376, 2019.

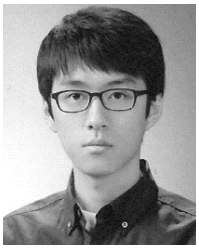

JOOYOUNG HONG received the B.S. degree in mechanical engineering from Yonsei University, in 2018. He is currently pursuing the M.S. degree in mechanical engineering with Seoul National University. His research interest includes robot mechanism design.

GARAM PARK received the B.S. degree in mechanical engineering from Hanyang University, in 2019, where he is currently pursuing the M.S. degree in mechanical engineering. His research interest includes robot mechanism design.

JISEOK LEE received the B.S. degree in mechanical engineering from Hanyang University, in 2019, where he is currently pursuing the M.S. degree in mechanical engineering. His research interest includes robot automatic control.

JONGWON KIM received the B.S. degree in mechanical engineering from Seoul National University, South Korea, in 1978, the M.S. degree in mechanical and aerospace engineering from the Korea Advanced Institute of Science and Technology (KAIST), South Korea, in 1980, and the Ph.D. degree in mechanical engineering from the University of Wisconsin–Madison, USA, in 1987. He is currently a Professor with the School of Mechanical and Aerospace Engineering, Seoul National University, South Korea. His current research interests include parallel mechanism, Taguchi methodology, and field robots.

HWA SOO KIM (M'15) received the B.S. and Ph.D. degrees in mechanical engineering from Seoul National University, South Korea, in 2000 and 2006, respectively. From 2007 to 2008, he was a Postdoctoral Researcher with the Laboratory for Innovations in Sensing, Estimation and Control, University of Minnesota, MN, USA. He is currently an Associate Professor with the Department of Mechanical System Engineering, Kyounggi University. His current research interests include design, modeling, and control of various mobile platforms.

TAEWON SEO (M'10) received the B.S. and Ph.D. degrees from the School of Mechanical and Aerospace Engineering, Seoul National University, South Korea. He was a Postdoctoral Researcher with the Nanorobotics Lab, Carnegie Mellon University, a Visiting Professor with Biomimetic Millisystems Lab, UC Berkeley, and an Assistant Professor with the School of Mechanical Engineering, Yeungnam University, South Korea. He is an Associate Professor with the School of Mechanical Engineering, Hanyang University, South Korea. His research interest includes robot design, analysis, control, optimization, and planning. He received the Best Paper Award from the IEEE/ASME TRANSACTIONS ON MECHATRONICS, in 2014. He is currently a Technical Editor of the IEEE/ASME TRANSACTION ON MECHATRONICS and an Associate Editor of the IEEE ROBOTICS AND AUTOMATION LETTERS and INTELLIGENT SERVICE ROBOTS.